Journal of the Korean Nuclear Society
Volume 36, Number 6, pp.512~527, December, 2004

Nonlinear Finite Element Analysis of Containment Vessel by Considering the Tension Stiffening Effect

Hong-Pyo Lee, Young-Sun Choun, and Jeong-Moon Seo
Korea Atomic Energy Research Institute
150, Deokjin-dong, Yuseong-gu, Daejeon, 305-353, Korea
hplee@kaeri.re.kr

Jae-Chul Shin
Chungnam National University
220, Gung-dong, Yuseong-gu, Daejeon, 305-764, Korea

(Received August 12, 2004)

Abstract

This paper describes the finite element (FE) analysis results of a 1/4 scale model of a pre-stressed concrete containment vessel (PCCV) by considering the tension stiffening effect, which is a result of the bond effect between the concrete and the steel. The tension stiffening model is assumed to be an exponential form based on the relationship between the average stress and the average strain of the concrete. The objective of the present FE analysis is to evaluate the ultimate internal pressure capacity of the PCCV, as well as its failure mechanism, when the PCCV model is subjected to a monotonous internal pressure beyond its design pressure capacity. With the commercial code ABAQUS, the FE analysis used two concrete failure criteria: a 2-dimensional axi-symmetric model with modified Drucker-Prager failure criteria and a 3-dimensional model with a damaged plasticity model. The results of our FE analysis on the ultimate pressure capacity and failure modes of PCCV have a good agreement with the experimental data.

Key Words : containment vessel, tension stiffening effect, 1/4 scale model, finite element analysis

1. Introduction

This paper describes the finite element (FE) analysis results of a 1/4 scale model of a pre-stressed concrete containment vessel (PCCV) tested by the Nuclear Power Engineering Corporation (NUPEC) of Japan and the U.S. Nuclear Regulatory Commission (NRC) [1]. The main objective of the present FE analysis is to evaluate the failure load of the PCCV as well as its failure mechanism when the PCCV model is subjected to a monotonous internal pressure

beyond its design pressure capacity of 0.39 MPa. In addition, we evaluate the performance of the existing numerical simulation tool and use the results as future numerical reference solutions.

Two FE models, a 2-dimensional axi-symmetric model and a 3-dimensional model with two penetrations and two buttresses, are considered in the present nonlinear FE analysis. In the axi-symmetric model, all the parts of the PCCV, such as the cylinder wall, dome, and basemat, are considered in the FE analysis. The concrete part was modeled with a 4-node axi-symmetric solid element and the steel liner was modeled with a 2-node axi-symmetric membrane element. In addition, the reinforcement and tendon were modeled with a rebar element. The Drucker-Prager model [2] is used for the concrete failure criterion to improve the numerical convergence problem after crack occurrence. In the 3-dimensional model, the concrete part was modeled with an 8-node solid element and the steel linear was modeled with a 4-node membrane element. The reinforcement and the tendon were modeled with the embedded element available in ABAQUS Ver. 6.3 [4]. A damaged plasticity model [3] is adopted for use as the concrete failure criterion to improve numerical convergence.

Once cracks are generated in the concrete, the anisotropy becomes significant so that the stress-strain relationship takes on an orthogonal anisotropy in a direction normal to the cracks. This means that the stress-strain relations have to be modeled respectively in directions that are parallel as well as normal to the cracks, and in the shear direction. Owing to the bond of the concrete to the reinforcing bars, the concrete continues to support a portion of the tensile force even after cracking has taken place in the reinforced concrete. This phenomenon is known as the tension stiffening effect. To simulate the tension stiffening effect, an exponential form based on the relationship between the average stress and the average strain of concrete is employed.

From the FE analysis, we found that the numerical results agree very well with the experimental data.

2. Constitutive Models

As mentioned, two FE models are prepared for the nonlinear analysis of a 1/4-scale PCCV model. One is a 2-dimensional axi-symmetric FE model and the other is a 3-dimensional FE model that considers penetrations such as an equipment hatch and personal airlock. This section describes the constitutive models used for these two FE models.

2.1. Concrete Model

2.1.1. 2-dimensional Axi-symmetric Model

The Drucker-Prager' s model [2] is used for the 2-dimensional axi-symmetric FE analysis. In this model, three different yield criteria based on the shape of the yield surface in the meridional plane are provided in ABAQUS. These yield surfaces are a linear form, a hyperbolic form, and a general exponent form. In the present analysis, a yield surface with a linear form is adopted. The linear model used in the FE analysis is written in terms of all three stress invariants:

$$F = t - p\tan\beta - d = 0 \tag{1}$$

where $t = \frac{1}{2}q\left[1+\frac{1}{K}-\left(1-\frac{1}{K}\right)\left(\frac{r}{q}\right)^3\right]$

p, q, r are stress invariants defined in the stress and strain measurements,

β is the slope of the linear yield and is commonly referred to as the friction angle of the material,

d is the cohesion of the material, and

K is the ratio of the yield stress in a tri-axial tension to the yield stress in a tri-axial compression and thus controls the dependency of the yield surface on the value of the intermediate principal stress.

Figure 1 shows the typical yield and flow surfaces of the linear model in the deviatoric plane. In this linear model, the flow is associated in the deviatoric plane, because the yield surface and the flow potential both have the same functional dependence on t. The values of $K=1$ and t=q imply that the yield surface is the von Mises circle in the deviatoric principal stress plane (the π-plane); in such a case, the yield stresses in a tri-axial tension and in a compression are the same. To ensure that the yield surface remains convex, $0.778 \leq K \leq 1.0$ is required. In the present FE analysis, the friction angle and the dilation angle are adopted as 71.56 degrees and 56.97 degrees, respectively [5].

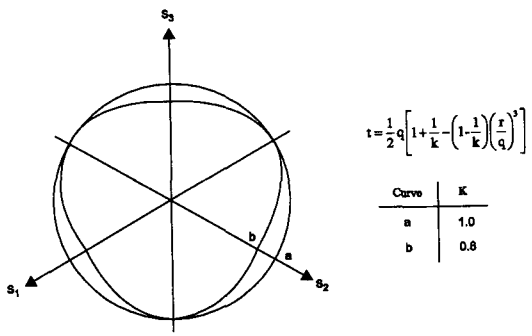

Fig. 1. Typical Yield and Flow Surfaces of the Linear Model in the Deviatoric Plane

2.1.2. 3-dimensional Model

The damaged plasticity model [3] is used for the concrete material in the 3-dimentional FE analysis. Specifically, two main failure mechanisms, the tensile cracking and compressive crushing of the concrete material, are considered in this model. The evolution of the yield (or failure) surface is controlled by two hardening variables related to failure mechanisms, $\overline{\varepsilon}_t^{pl}$ and $\overline{\varepsilon}_c^{pl}$, which are the tensile and compressive equivalent plastic strains, respectively.

In this model, the uni-axial tensile and compressive response of concrete is characterized by the damaged plasticity model shown in Figure 2. Under uni-axial tension, the stress-strain relationship follows a linear elastic relationship until it reaches the value of the failure stress (σ_{t0}). The failure stress corresponds to the onset of micro-cracking in the concrete material. Beyond the failure stress, the formation of micro-cracks is represented macroscopically with a softening stress-strain response, which induces strain localization in the concrete structure. Under uni-axial compression, the response is linear until the value of the initial yield (σ_{c0}) is reached. In the plastic regime, the response is typically characterized by a stress hardening followed by a strain softening beyond the ultimate stress σ_{cu}.

It is assumed that the uni-axial stress-strain curves can be converted into stress-strain versus plastic-strain curves. Thus,

$$\sigma_t = \sigma_t\left(\overline{\varepsilon}_t^{pl}, \dot{\overline{\varepsilon}}_t^{pl}, \theta, f_i\right)$$
$$\sigma_c = \sigma_c\left(\overline{\varepsilon}_c^{pl}, \dot{\overline{\varepsilon}}_c^{pl}, \theta, f_i\right) \quad (2)$$

where the subscripts t and c refer to the tension and compression, respectively. $\overline{\varepsilon}_t^{pl}$ and $\overline{\varepsilon}_c^{pl}$ are the equivalent plastic strains and $\dot{\overline{\varepsilon}}_t^{pl}$ and $\dot{\overline{\varepsilon}}_c^{pl}$ are the corresponding plastic strain rates. θ is the temperature and $f_i (i=1,2,\cdots)$ are the other predefined field variables.

As shown in Figure 2, when the concrete specimen is unloaded from any point onto the strain softening branch of the stress-strain curves, the unloading response is weakened and the elastic stiffness of the material appears to be damaged (or degraded). The degradation of the elastic stiffness is characterized by two damage variables, d_t and d_c, which are assumed to be functions of the plastic

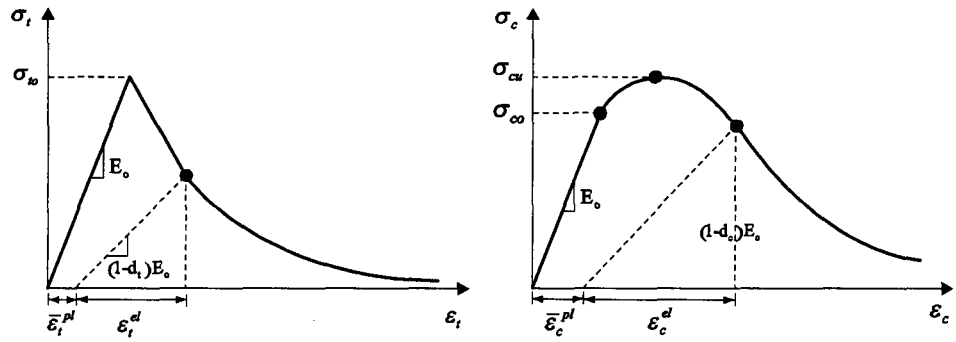

Fig. 2. Response of Concrete to Uniaxial Loading in Tension(left) and Compression(right)

strains, temperature, and field variables:

$$d_t = d_t\left(\bar{\varepsilon}_t^{pl}, \theta, f_i\right); \quad 0 \le d_t \le 1$$
$$d_c = d_c\left(\bar{\varepsilon}_c^{pl}, \theta, f_i\right); \quad 0 \le d_c \le 1 \tag{3}$$

The damage variables can take values from zero, representing the undamaged material, to one, which represents a total loss of strength. If is the initial (undamaged) elastic stiffness of the material, the stress-strain relations under uni-axial tension and compression load are:

$$\sigma_t = (1-d_t)E_0\left(\varepsilon_t - \bar{\varepsilon}_t^{pl}\right)$$
$$\sigma_c = (1-d_c)E_0\left(\varepsilon_c - \bar{\varepsilon}_c^{pl}\right) \tag{4}$$

2.2. Tension Stiffening Model

Owing to the bond effect between the concrete and reinforcing bars, the concrete can withstand some of the tensile force even after crack formation. This means that the stiffness of the reinforced concrete remains higher than that of the reinforcing bars alone. This phenomenon is called the tension stiffening effect. In a numerical simulation, this effect can be represented by either modifying the stiffness of the reinforcing bars or by modifying the stiffness of the concrete so that the concrete can carry the tensile force after cracking. In the present FE analysis, the latter tension-stiffening model, which was proposed by Okamura [6], is adopted (see Figure 3).

From Okamura' s study,

Ascending branch ($\varepsilon_t \le \varepsilon_{cr}$):

$$\sigma_t = E_c \cdot \varepsilon_t \tag{5}$$

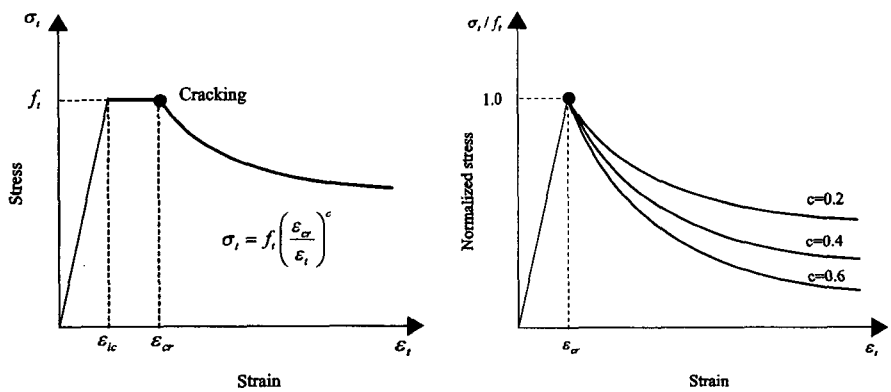

Fig. 3. Tension Stiffening Model (left) and Tension Stiffening Parameter (right) for Concrete

Descending branch ($\varepsilon_t > \varepsilon_{cr}$):

$$\sigma_t = f_t \left(\frac{\varepsilon_{cr}}{\varepsilon_t} \right)^{0.2} \quad (6)$$

Where ε_t is the total strain of the concrete, ε_{cr} is the cracking strain and f_t is the tensile strength of the concrete. ε_{cr} is $2 \cdot \varepsilon_{ic} = 2 \cdot (f_t/E)$, as proposed by Okamura. E is the elastic modulus of the concrete. Superscript c, which is dependent on the used steel type, is the tension stiffening parameter, as shown in Figure 3 (right). Usually, the tension stiffening parameters of the welded wire mesh, deformed bar, and round bar are 0.2, 0.4, and 0.6, respectively.

2.3. Reinforcing Steel Model

The stress-strain relationship of mild steel is usually assumed to be elasto-plastic with a distinct yield stress of f_y. However, when the reinforcing bars are surrounded by concrete, the average stress-strain relationship exhibits very different behavior than that exhibited by a bare bar without concrete, as shown in Figure 4. To consider this behavior, we generally underestimate the yield stress. This is the apparent yield stress of a embedded bar in concrete. In the present FE analysis, the apparent yield stress for this situation

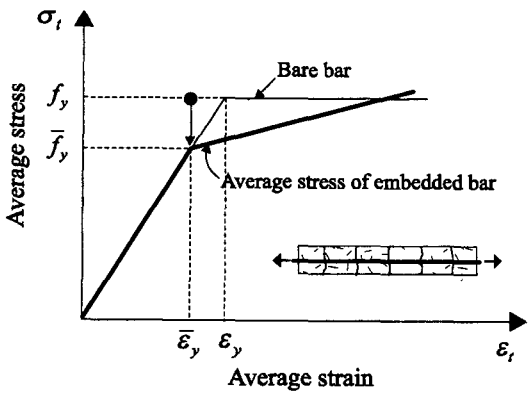

Fig. 4. Average Yield Stress-Strain Curve

is represented by Hsu' s model [7] as follows:

$$\frac{\bar{f}_y}{f_y} = 1 - \frac{4}{\rho} \left(\frac{f_{cr}}{f_y} \right)^{1.5} \quad (7)$$

Where f_y and $\bar{f}_y$ are the yield stresses of the bare bar and the embedded bar in concrete, respectively. ρ is the reinforcement ratio and f_t is the cracking stress value, as mentioned in equation (6).

2.4. Liner Plate and Tendon Model

The stress-strain curve for the liner plate and tendon are generally assumed to be identical for tension and compression. For simplicity in a numerical analysis, the liner plate and tendon are idealized by a one-dimensional stress-strain relationship. In this study, the stress-strain curve for the liner plate and tendon is modeled by using an elasto-plastic material model that is available in ABAQUS Ver. 6.3. The von Mises failure criteria with isotropic hardening are adapted to represent the nonlinear behavior of the materials.

3. Material Properties used in FE Analysis

The material properties for the concrete, steel rebars, post-tensioned tendons, and steel liner are prepared by using the experiment data provided by Sandia National Laboratories (SNL) [1]. In this section, the material properties used in the FE analysis are briefly described.

3.1. Geometrical Definition

The PCCV model is a uniform 1/4 scale model of a pre-stressed concrete cylindrical shell with a hemispherical dome and a continuous steel liner anchored to a reinforced concrete basemat that extends beyond the containment to support other plant structures. The model includes a scaled

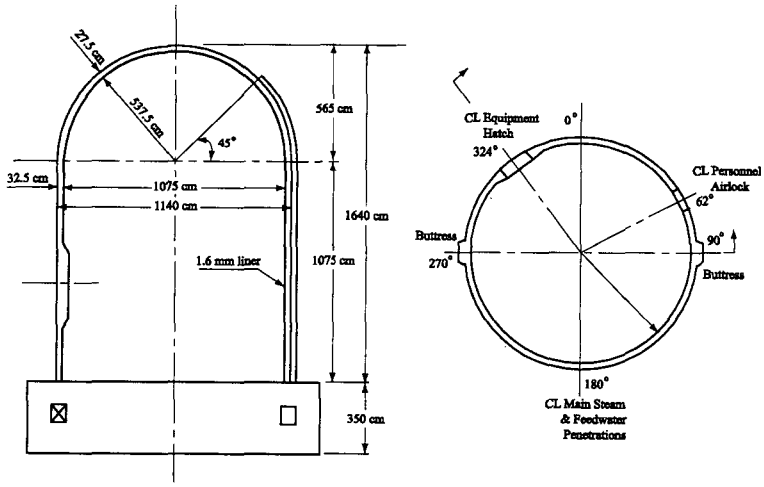

Fig. 5. Geometrical Shape of the PCCV Model

representation of the equipment hatch, the personal airlock, and the main steam and feedwater line penetrations. The design pressure capacity of this prototype containment vessel is 0.39 MPa.

The overall geometry and dimensions of the PCCV model are shown in Figure 5.

3.2. Concrete

Two types of concrete, normal strength concrete and high strength concrete, were used to construct the SNL PCCV test model [1]. In the present FE analysis, the material property data for the trial mix concrete based on field curing are

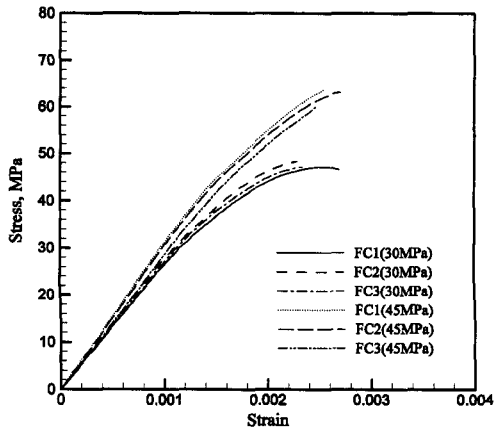

Fig. 6. Stress-Strain Curve for Concrete

Table 1. Material Data for the Trial Mix Concrete (Unit: MPa)

Material / Item	fc′ =29.42 (basemat)		fc′ =44.13 (dome & wall)	
	Standard Curing (SC)	Field Curing (FC)	Standard Curing (SC)	Field Curing (FC)
Compressive strength	51.39	41.68	60.21	48.84
Tensile strength	3.93	3.37	4.21	3.45
Flexural strength	5.37	4.00	5.58	5.51
Young' s modulus	29,030	27,950	31,970	26,970
Poisson' s ratio	0.20	0.18	0.20	0.18
Density (ton/m^3)	2.25	2.21	2.26	2.19

used. The stress-strain curve is illustrated in Figure 6. The material properties adopted in the FE analysis are described in Table 1.

3.3. Reinforcing Steel

The material properties for each type of rebar are selected from the test data. The material properties are summarized in Table 2 and the test data for the reinforcing bar is illustrated in Figure 7(a) [1]. In the FE analysis, we adopt the mean value for the material properties of the rebar.

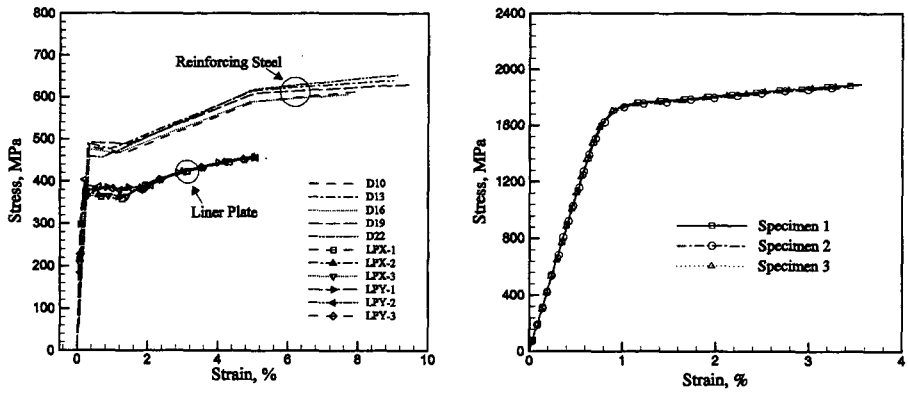

(a) Reinforcing Steel and Liner Plate **(b) Tendon**

Fig. 7. Stress-strain Curve for the Steel

Table 2. Material Properties for the Reinforcing Steel (Unit: MPa)

Item \ Material	D10	D13	D16	D19	D22
Elastic modulus	1.83E5	1.83E5	1.83E5	1.84E5	1.91E5
Poisson' s ratio	0.3	0.3	0.3	0.3	0.3
Yield stress	482.0	490.1	476.6	491.9	459.0
Ultimate stress	613.6	640.4	606.2	630.4	653.2
Elongation (%)	20.5	24.2	22.1	21.1	18.7

Table 3. Material Properties for the Steel Liner (Unit: MPa)

Material	Test sample	Yield stress	Ultimate stress	Elongation(%)
SGV410	LPY-1	381.5	495.2	33.8
〃	LPY-2	403.1	498.2	33.0
〃	LPY-3	385.4	497.2	33.6
〃	LPX-1	377.6	499.2	33.0
〃	LPX-2	377.6	500.1	33.0
〃	LPX-3	370.7	497.2	33.0
Average		382.7	497.85	33.2

3.4. Liner Plate

Two sets of material samples for the steel liner plate, LPY in a vertical direction and LPX in a circumferential direction, were tested to evaluate their material properties. Each test set consisted of three samples. The stress-strain data is illustrated in Figure 7(a) and the test results are summarized in Table 3.

3.5. Tendon

The ultimate stress and strain test data of the tendon are shown in Table 4. Tendon strain data is calculated from the information obtained from SNL by testing both individual tendon assemblies according to two Japanese test standards, JISG 3536 and JISZ 2241. The engineering stress-strain data, plotted in Figure 7(b), indicates that almost identical test results were obtained for the three samples shown. The stress results were obtained by dividing the measured forces by the initial cross sectional area of 339 mm^2 for each tendon.

Table 5 shows the pre-stressing data summary, prepared by SNL, which tabulates the averages for the measurements of the forces, friction, and seating losses. In this study, an average final load cell force that includes the different pre-stressing losses is adopted for the tendon.

Table 4. Material Properties for the Tendon

Test specimen	Ultimate stress (MPa)	Failure strain (%)
Specimen 1	1,924	3.32
Specimen 2	1,912	3.51
Specimen 3	1,932	3.36
Mean	1,922.6	3.39

Table 5. Pre-stressing Data Summary

Item	Hoop tendons		Vertical tendons	
Average tensile force:				
design:	44.41 Ton	97.9 kips	49.57 Ton	109.00 kips
jack:	43.53 Ton	95.97 kips	49.02 Ton	106.27 kips
load cell:	43.21 Ton	95.27 kips	48.20 Ton	108.07 kips
Average lift-off force:				
design:	34.11 Ton	75.2 kips	46.31 Ton	102.10 kips
jack:	34.02 Ton	75.01 kips	44.22 Ton	97.49 kips
Average friction coefficient:	0.18		0.22	
Average seating loss:				
jack:	9.51 Ton	20.96 kips	4.80 Ton	10.58 kips
load cell:	9.86 Ton	21.75 kips	4.64 Ton	10.23 kips
Average final load cell force:	33.34 Ton	73.52 kips	43.56 Ton	96.04 kips

3.6. Limit State Test and Structural Failure Mode Test

The Limit State Test (LST)[8] was designed to fulfill the primary objectives of the PCCV test program, i.e., to investigate the response of representative models of nuclear containment structures in an accident situation in which pressure loading exceeds the design parameters, and to compare analytical predictions with measured behavior. During the LST, the pressure was increased to slightly over 3.3Pd before the leak rate exceeded the capacity of the pressurization system. After the model pressure was reduced to 1.0Pd, test personnel were able to carefully inspect the model for evidence of concrete cracking. There was no indication of tendon or rebar failure after LST.

Almost immediately after the completion of the LST, a Structural Failure Mode Test (SFMT) was conducted to observe the structural failure mode of the PCCV. The model was filled with water to 1.5m from the dome apex, which is approximately 97% of the interior volume of the vessel. The SFMT sequence used nitrogen gas to compensate for the known leaks in the model. The model was rapidly pressurized, up to rupture, and the collapse was recorded with digital video cameras.

3.7. FE Analysis Procedure for the ABAQUS Code

The numerical analysis steps used in the present FE analysis are:

(1) Gravity + Pre-stress force

(2) Gravity + Pre-stress force + Internal pressure

An initial load step is established in which the PCCV is brought into a static equilibrium with the initial post-tensioning tendon loads and self-weight. The weight of the embedded steel reinforcements and tendons has not been included as part of the total containment vessel weight.

After an initial load step, a uniform pressure is applied to the face of the liner plate elements that comprise the internal surface of the vessel. Internal pressure is also applied to the penetration cover plates, such as in the personal airlock and equipment hatch.

4. Finite Element Model

4.1. 2-dimensional Axi-symmetric Model

The axi-symmetric FE model used in the prediction of the overall response of the PCCV is illustrated in Figure 8. The FE model consists of 768 axi-symmetric 4-node solid elements (CAX4) to represent the concrete layer and 203 axi-symmetric 2-node membrane elements (MAX1) to represent the liner layer, as shown in Figure 8. All the rebars and tendons are modeled by using the rebar sub-element provided in the code ABAQUS.

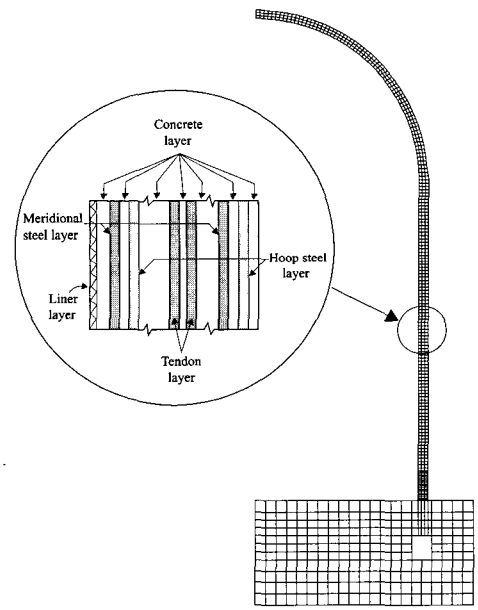

Fig. 8. Axi-symmetric Finite Element Model

Therefore, they are assumed to be rigidly bonded to the concrete. The pre-stressing force for the tendon is represented by the *INITIAL CONDITION option in ABAQUS. The boundary condition for the bottom of the base slab is assumed to be fixed, so the present FE model can not simulate a possible vertical uplift during internal pressurization.

4.2. 3-dimensional Model

A 3-dimensional FE model with large penetrations such as an equipment hatch and an air lock is also adopted, as shown in Figure 9. The 3-dimensional model consists of 6,992 8-node solid elements (C3D8), 3,100 4-node liner elements (M3D4), and 9,522 truss elements (T3D3). The rebar and tendon are modeled with an embedded element. The layout of the tendon used in the present FE analysis is illustrated in Figures 9 (c) and (d). The pre-stressing force for the tendon is represented by the *INITIAL CONDITION option in ABAQUS. Because of difficulty in FE mesh generation, the tendons are assumed to remain rigidly bonded to the concrete. Therefore, to simplify the analysis procedure, the slippage of a tendon within the tendon sheath is not considered in the present FE analysis model. Consequently, the effect of bond between the concrete and the steel is neglected in this study.

The boundary condition for the bottom of the base slab is assumed to be fixed, similar to that used in the axi-symmetric model, so this model is also unable to simulate a possible vertical uplift during internal pressurization.

5. FE Analysis Results

5.1. Tension Stiffening Effect

From the 2-dimensional axi-symmetric analysis result, Figures 10, 11, and 12 show the pressure-displacement curve due to tension stiffening parameters for the mid-height of the wall, the spring-line, and the apex of the dome, respectively, where c=0.2, 0.4, and 0.6, respectively [5].

As shown in the Figures, nonlinear FE analysis results of the containment are significantly influenced by the tension stiffening effect. The higher the tension stiffening parameter used, the lower the predicted ultimate pressure capacity of the PCCV. That is, when the tension stiffening parameter is 0.6, the ultimate pressure capacity of

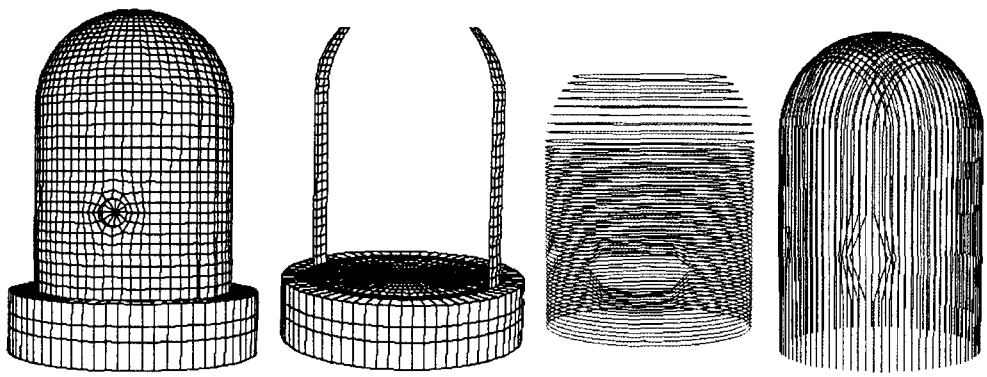

Fig. 9. 3D FE Mesh: (a) Full Model (b) Buttress and Basemat (c) Hoop Tendon (d) Meridional Tendon

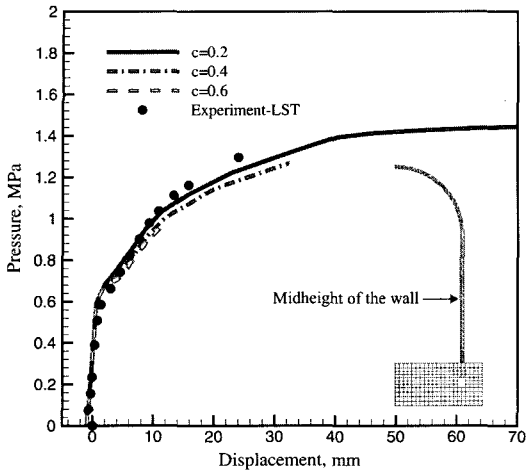

Fig. 10. Radial Displacement due to Tension Stiffening Effect at the Mid-height of the Wall

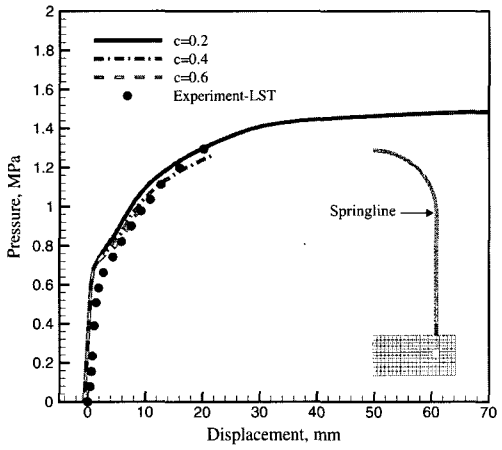

Fig. 11. Radial Displacement due to Tension Stiffening Effect at Springline

the PCCV is 2.5 times higher than the design pressure level. In this case, cracking of concrete and yielding of steel reinforcement occur to some extent, but yielding of the tendon does not occur at any position.

Consequently, as shown in Figures 10 through 12, it is found that the FE analysis results are in good agreement with the experimental data when

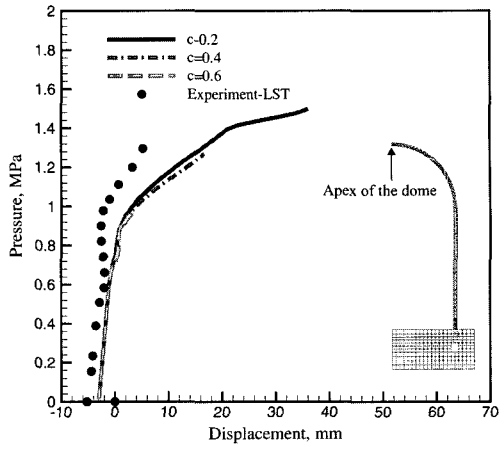

Fig. 12. Vertical Displacement due to Tension Stiffening Effect at Dome Apex

the tension stiffening parameter is 0.2 because of the high steel ratio of the PCCV. So, 0.2 is used as the tension stiffening parameter in the following 2-dimensional axi-symmetric and 3-dimensional FE nonlinear analyses.

5.2. Axi-symmetric Analysis Results

The first cracking of the concrete in the cylinder wall due to hoop stress occurred at 0.59 MPa in the cylinder. The cracking of the cylinder due to meridional stress is initiated at the same pressure level at the mid-height of the cylinder wall. Then, at 0.67 MPa, cracks spread all over the cylinder of the PCCV. The cracking of the concrete caused a sudden change in the stiffness of the structure. Beyond this point, the tendons and reinforcing steels have to sustain the internal pressure.

The first crack occurs in the lower part of the dome and the cracks are observed at 0.67 MPa and 0.77 MPa in the upper part of the dome.

The first yielding of the hoop rebar is initiated at 1.036 MPa at the mid-height of the cylinder wall, and the yielding of the meridional rebar in the wall-basemat junction began at 1.29 MPa. The

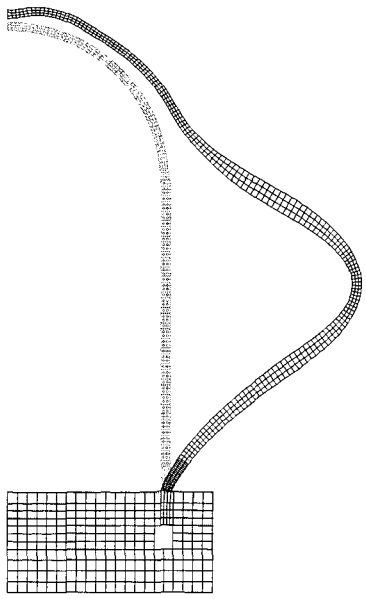

Fig. 13. Deformed Shape of Axi-symmetric Model at Ultimate Pressure(× 100)

maximum strain of the rebar in the hoop direction is observed as 14.37% at the mid-height of the cylinder wall at the final stage.

The strain values of the hoop tendons in a cylinder wall reach 1%, 2%, and 3% for stress values of 1.43 MPa, 1.47 MPa, and 1.50 MPa, respectively. The maximum strain of the hoop tendon in a cylinder wall is observed as 15.26% at the final stage.

The deformed shape of the axi-symmetric model at the ultimate pressure state is shown in Figure 13.

5.3. 3-dimensional Analysis Results

The deformed shape of the 3-dimensional model at the ultimate pressure state is illustrated in Figure 14. The deformation is very irregular around penetrations, like an equipment hatch or airlock, and around buttresses, due to geometric discontinuity. This geometric discontinuity may affect the overall behavior and ultimate pressure capacity of the PCCV. Therefore, it is shown that the penetrations and the buttresses have to be taken into account during a nonlinear FE analysis of the PCCV to improve the accuracy and reliability of the analysis results.

The first hoop and meridional cracking of the cylinder wall occurred at 0.62 MPa, as shown in Figure 15. This is a larger pressure value than the corresponding cracking pressure obtained from the axi-symmetric model. The first crack occurs at the lower part of the dome and cracks are also observed at the upper part of the dome at values of 0.675 MPa and 1.06 MPa.

The first yielding of the hoop rebar is initiated at 0.94 MPa at the mid-height of the cylinder wall, as shown in Figure 16, and yielding of the meridional rebar in the wall-basemat juncture began at 1.19 MPa. The maximum strain of the hoop rebar is observed at the mid-height of the cylinder wall with a value of 0.55% at the final stage. The maximum value of the strain in the hoop tendon is observed as 0.51% at the final stage. Because a numerical instability has occurred, there is no indication of a tendon or rebar failure at the final load step.

Displacement verses internal pressure relationship comparisons at several Standard Output Locations (SOLs), such as at mid-height of the cylinder, spring-line, and dome apex, are shown in Figures 17 through to 20. There is very good agreement between the analysis and test results for vertical displacement in the spring-line (Figure 19) as well as for radial displacement at the mid-height of the cylinder (Figure 17) and at the spring-line (Figure 18).

Maximum displacement is observed at the mid-height of the cylinder El. 6.2m. From the test results, the value of the maximum displacement for the radial direction is 2.3cm by the Limit State Test (LST) and 8.498cm by the Structural Failure

Table 6. Pressure Level due to the Event Milestones (Unit: MPa)

Event milestones	Axi-sym. model	3D model
First cracking of concrete in cylinder due to hoop stress	0.59	0.62
First cracking of concrete in cylinder due to meridional stress	0.59	0.62
First yield of hoop rebar in cylinder	1.036	0.94
First yield of meridional rebar in wall-basemat juncture	1.29	1.19
First cracking of dome concrete above 45° dome angle	0.77	1.06
First cracking of dome concrete below 45° dome angle	0.67	0.675
Hoop tendons in cylinder reaching 1% strain	1.43	-
Hoop tendons in cylinder reaching 2% strain	1.47	-
Hoop tendons in cylinder reaching 3% strain	1.50	-

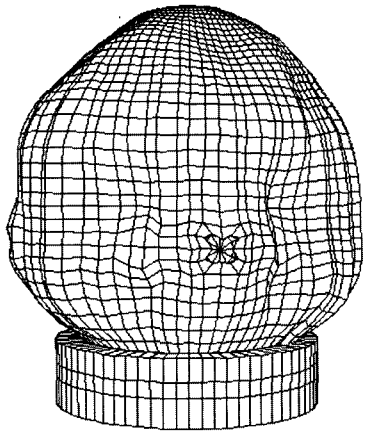

Fig. 14. Deformed Shape of 3D Model at Ultimate Pressure(× 100)

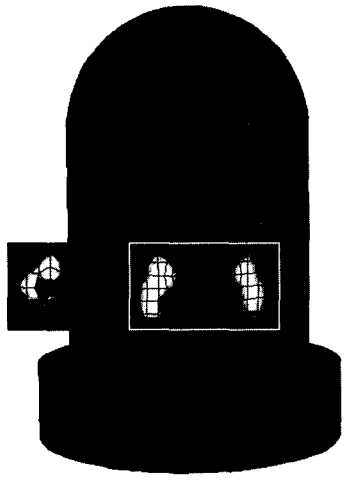

Fig. 15. The First Crack Location of the Concrete

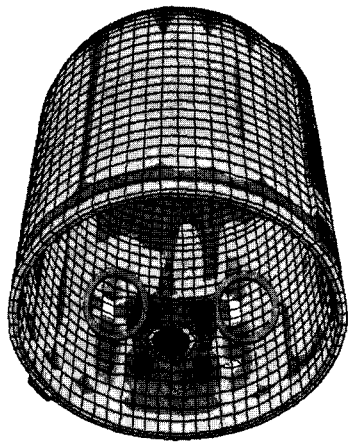

Fig. 16. The First Yielding Location of the Rebar

Mode Test (SFMT) at the final load stage. From the 3-dimensional FE analysis results, the value of the maximum displacement for the radial direction is 3.0 cm at the final load stage, which is very similar to the value determined by the experimental data.

As mentioned above, the first crack occurred at 0.62 MPa. The analysis and the test consistently exhibit a sharp jump in displacement at the cracking pressure. There is a poor correlation between the analysis and the test data for vertical displacement in the dome apex. Unfortunately, the test data of the LST and the SFMT are quite different.

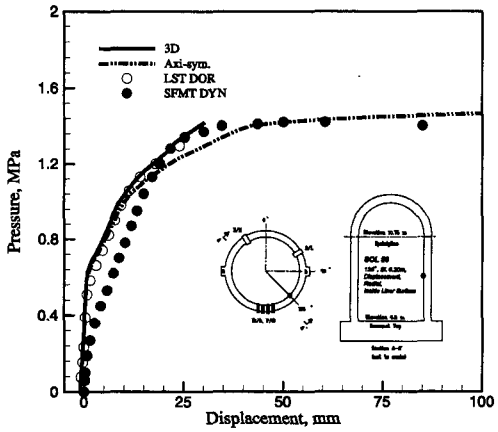

Fig. 17. Radial Displacement at the Mid-height of the Cylinder

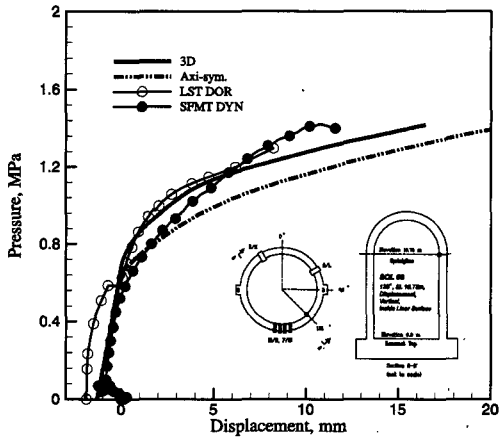

Fig. 19. Vertical Displacement at Spring-line

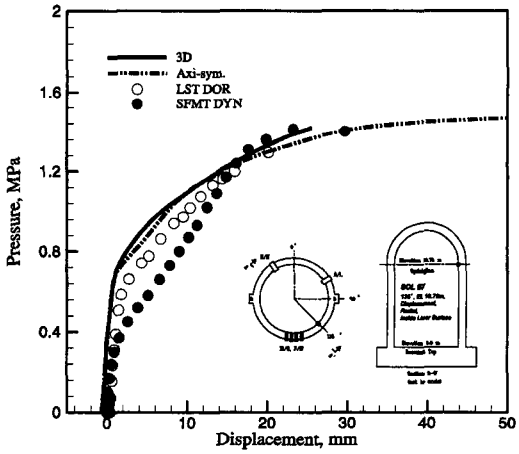

Fig. 18. Radial Displacement at Spring-line

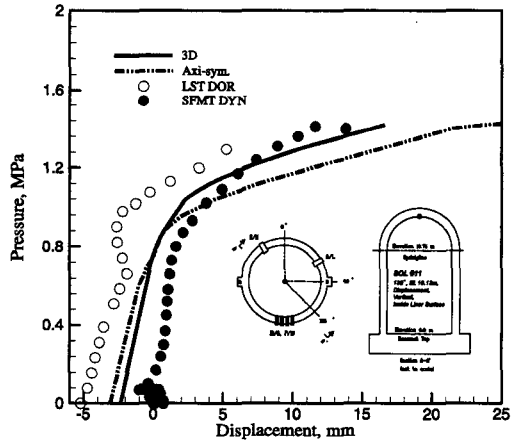

Fig. 20. Vertical Displacement at Dome Apex

Finally, The pressure levels due to the event milestones requested by SNL are summarized in Table 6.

5.4. Ultimate Pressure Capacity

One important aspect of the PCCV model response in the high pressure tests is the concept of a failure. There are two failure criteria: one is functional failure, the other is structural failure. Functional failure for the prototypical containment is defined in the regulations as containment leak rates exceeding 0.1 to 0.5% of the containment mass per day due to a liner tearing. The functional failure criteria are not particularly useful for testing the structural capacity of a containment vessel model, especially when one of the objectives is to generate large inelastic response modes for a comparison with the analytical predictions, which may be well beyond the levels required to cause a functional failure. Structural failure is defined in terms of local strain measurements of an individual structural element (i.e., liner, rebar, tendon, and concrete) exceeding the maximum strain level.

Predictions of the ultimate internal pressure capacity of a vessel have often been based on the structural failure of the tendon used in its construction. When the local strain of the tendon exceeds 3%, it is assumed that a structural failure of the PCCV has occurred. Experimentally, the PCCV model ruptured violently with the breaking of a tendon wire near the mid-height of the cylinder at 1.452 MPa (3.63Pd) which is, as mentioned, greater than the accepted ultimate internal pressure due to a structural failure.

The results of the nonlinear FE analysis show that a structural failure occurred near the mid-height of the cylinder at 1.5 Mpa. This indicates that the ultimate pressure of the PCCV is similar to the FE analysis and the empirical test. Consequently, the safety margin for the ultimate internal pressure of the PCCV is 3.6 times higher than the design pressure level.

6. Conclusions

In this study, a nonlinear finite element analysis of a 1/4 scale model of a pre-stressed concrete containment vessel was conducted to predict the ultimate internal pressure capacity. From the finite element analysis results, the following conclusions were obtained.

1) Initial concrete cracking was observed at a pressure of 0.52 MPa (axi-symmetric model) and 0.62 MPa (3-dimensional model) at the cylinder wall. The cracking of the concrete caused a sudden change in the stiffness of the structure. Beyond this point, tendons and reinforcing steels have to sustain the internal pressure.
2) Location of the maximum displacement is at the mid-height of the cylinder wall, which is the critical section of the PCCV. The value of a maximum displacement is 2.3cm and 3.0cm for the experimental result (LST) and FE analysis result (3D), respectively, at the final load stage.
3) The deformed shape of the 3-dimensional model is very irregular around penetrations (e.g., an equipment hatch or airlock) and buttresses due to geometric discontinuity. So, an axi-symmetric result cannot be achieved. Geometric discontinuity may affect the overall behavior and ultimate pressure capacity of the PCCV. Therefore, it is shown that penetrations and buttresses have to be taken into account during a nonlinear FE analysis of the PCCV to improve the accuracy and reliability of the analysis results.
4) Structural failure of the PCCV due to a tendon rupture occurred at 1.5 MPa, near the mid-height of the cylinder wall. This failure occurred at a pressure 3.5 times higher than the stated design pressure of 0.39 MPa.

Acknowledgements

This research was supported by the Mid- and Long-Term Nuclear Research & Development Program of the Ministry of Science and Technology, Korea.

References

1. Dameron, R.A., Hansen, R.A., Parker, D.R. and Rashid, Y.R., Posttest Analysis of the NUPEC/NRC 1:4 Scale Prestressed Concrete Containment Vessel Model, NUREC/CR-6809, (1998).
2. Drucker, D.C. and Prage W., Soil Mechanics and Plastic Analysis or Limit Design, Quarterly of Applied Mathematics, Vol. 10, pp. 157-165 (1951).
3. Lee, J. and Fenves G.L., Plastic-Damaged Model for Cyclic Loading of Concrete Structures, Journal of engineering mechanics, Vol. 124, No. 8, pp. 892-900 (1998).

4. Hibbit, H.D., ABAQUS User's Manual, Version 6.3, HKS Inc., (2002).
5. Moon, I.H. and Sim, J.S, An Ultimate Pressure Capacity Assessment of Prestressed Concrete Containment Vessel Considering Non-symmetric Factors, KSCE, Vol. 24, No.3A, pp. 639-646, (2004).
6. Okamura, H., Maekawa K. and Sivasubramaniyam S., Verification of Modeling for Reinforced Concrete Finite Element, Finite Element Analysis of Reinforced Concrete Structures, ASCE, pp. 528-543, (1985).
7. Hsu, T.T.C. and Belarbi A., Constitutive Laws of Concrete in Tension and Reinforcing Bars Stiffened by Concrete, ACI Structural Journal, Vol. 91, No. 4, pp. 465-474, (1994).
8. Hessheimer, M.F., Klamerus, E.W., Lambert, L.D. and Rightley, G.S., Overpressurization Test a 1:4 Scale Prestressed Concrete Containment Vessel Model, Sandia National Laboratories, NUREG/CR-6810, (2003).